J|A|C|S
ARTICLES
Published on Web 05/12/2007

Transition State Analysis of Acid-Catalyzed dAMP Hydrolysis

Joe A. B. McCann‡ and Paul J. Berti*,†, ‡

Contribution from the Department of Chemistry and Department of Biochemistry and Biomedical Sciences, McMaster University, 1280 Main Street West, Hamilton, ON, L8S 4M1, Canada

Received October 13, 2006; E-mail: berti@mcmaster.ca

Abstract: Multiple kinetic isotope effects (KIEs) on deoxyadenosine monophosphate (dAMP) hydrolysis in 0.1 M HCl were used to determine the transition state (TS) structure and probe its intrinsic reactivity. The experimental KIEs revealed a stepwise (S_N1) mechanism, with a discrete oxacarbenium ion intermediate. This is the first direct evidence for the deoxyribosyl oxacarbenium ion in solution. In 50% methanol/0.1 M HCl the products were deoxyribose 5-phosphate (dRMP) and α- and β-methyl dRMP. The α-Me-dRMP/β-Me-dRMP ratio was 8.5:1. Assuming that a free oxacarbenium ion is equally susceptible to nucleophilic attack on either face, this indicated that ~20% proceeded through a solvent-separated ion pair complex, or free oxacarbenium ion, a $D_N + A_N$ mechanism, while ~80% of the reaction proceeded through a contact ion pair complex. The oxacarbenium ion lifetime was estimated at 10^{-11}–10^{-10} s. Computational transition states were found for A_ND_N, $D_N^{\ddagger}{*}A_N$, $D_N{*}A_N^{\ddagger}$, and $D_N + A_N$ mechanisms using hybrid density functional theory calculations. After taking into account 20% of $D_N + A_N$, there was an excellent match of calculated to experimental KIEs for 80% of the reaction having a $D_N{*}A_N^{\ddagger}$ mechanism. That is, C–N bond cleavage is reversible, with dAMP and the {oxacarbenium ion•adenine} complex in equilibrium. The first irreversible step is water attack on the oxacarbenium ion. The calculated 1′-^{14}C KIE for a stepwise mechanism with irreversible C–N bond cleavage ($D_N^{\ddagger}{*}A_N$) was 1.052, in the range previously associated only with A_ND_N transition states, and close to the calculated A_ND_N value, 1.059. The 1′-^{14}C KIE was strongly dependent on the adenine protonation state.

Enzymatic mechanisms reflect an interplay between the substrates' intrinsic reactivities and catalytic strategies to lower activation energies. Transition state (TS[1]) analyses of nonenzymatic 2′-hydroxynucleoside hydrolysis have demonstrated their intrinsic reactivities,[2−4] while TS analyses of enzymatic[3,5−10] reactions have revealed the catalytic strategies used to promote those reactions. For 2′-deoxynucleosides, three enzymatic TS analyses have been reported[11−14] but no nonenzymatic reactions until now. As noted recently,[15,16] this deficiency impedes understanding the enzymatic transition states. TS analysis of nonenzymatic reactions reveals the catalytic imperative and helps identify potentially effective catalytic strategies. 2′-Deoxynucleoside reactivity is relevant to DNA base excision repair, nucleoside metabolism, and spontaneous DNA depurination.[15,17,18]

"TS analysis" is the use of multiple kinetic isotope effects (KIEs) to determine TS structures.[19,20] KIEs report on changes in bond stretching and bending forces between the reactant and

† Department of Chemistry.
‡ Department of Biochemistry and Biomedical Sciences.

(1) Abbreviations: α-, β-Me-dRMP, α- or β-methyl deoxy-D-ribose-5′-monophosphate; APRTase, adenine phosphoribosyl transferase; CIPC, contact ion pair complex; cpm, counts per min; dAdo, deoxyadenosine; DFT, density functional theory; dRMP, deoxy-D-ribose-5′-monophosphate; DTT, dithiothreitol; EIE, equilibrium isotope effect; *f*, fractional extent of reaction; KIE, kinetic isotope effect; MK, myokinase; MTAN, 5′-methylthioadenosine/*S*-adenosylhomocysteine nucleosidase; n_{ij}, Pauling bond order; PEP, phospho*enol*pyruvate; PK, pyruvate kinase; PRPPase, phosphoribosyl pyrophosphate synthetase; $Q,Q^{\ddagger}$, reduced isotopic partition function; RTRase, ribonucleoside triphosphate reductase; SSIPC, solvent separated ion pair complex; TBAS, tetrabutylammonium hydrogen sulfate; TEAA, triethyl ammonium acetate; $\theta_{H2'}$, dihedral angle of p-orbital–C1′–C2′–H2′; TP, thymidine phosphorylase; TS, transition state; UDG, uracil DNA glycosylase.

(2) Berti, P. J.; Schramm, V. L. *J. Am. Chem. Soc.* **1997**, *119*, 12069−12078.
(3) Mentch, F.; Parkin, D. W.; Schramm, V. L. *Biochemistry* **1987**, *26*, 921−930.
(4) Parkin, D. W.; Leung, H. B.; Schramm, V. L. *J. Biol. Chem.* **1984**, *259*, 9411−9417.
(5) Chen, X.-Y.; Berti, P. J.; Schramm, V. L. *J. Am. Chem. Soc.* **2000**, *122*, 1609−1617.
(6) Berti, P. J.; Blanke, S. R.; Schramm, V. L. *J. Am. Chem. Soc.* **1997**, *119*, 12079−12088. Kline, P. C.; Schramm, V. L. *Biochemistry* **1995**, *34*, 1153−1162. Scheuring, J.; Berti, P. J.; Schramm, V. L. *Biochemistry* **1998**, *37*, 2748−2758. Scheuring, J.; Schramm, V. L. *Biochemistry* **1997**, *36*, 4526−4534. Scheuring, J.; Schramm, V. L. *Biochemistry* **1997**, *36*, 8215−8223. Rising, K. A.; Schramm, V. L. *J. Am. Chem. Soc.* **1997**, *119*, 27−37. Horenstein, B. A.; Parkin, D. W.; Estupinan, B.; Schramm, V. L. *Biochemistry* **1991**, *30*, 10788−10795. Parkin, D. W.; Mentch, F.; Banks, G. A.; Horenstein, B. A.; Schramm, V. L. *Biochemistry* **1991**, *30*, 4586−4594. Kline, P. C.; Schramm, V. L. *Biochemistry* **1993**, *32*, 13212−13219. Parikh, S. L.; Schramm, V. L. *Biochemistry* **2004**, *43*, 1204−1212.
(7) Bates, C.; Kendrick, Z.; McDonald, N.; Kline, P. C. *Phytochemistry* **2006**, *67*, 5−12. Hunt, C.; Gillani, N.; Farone, A.; Rezaei, M.; Kline, P. C. *Biochim. Biophys. Acta* **2005**, *1751*, 140−149.
(8) Parkin, D. W.; Schramm, V. L. *Biochemistry* **1987**, *26*, 913−920.
(9) Singh, V.; Lee, J. E.; Nunez, S.; Howell, P. L.; Schramm, V. L. *Biochemistry* **2005**, *44*, 11647−11659.
(10) Lewandowicz, A.; Schramm, V. L. *Biochemistry* **2004**, *43*, 1458−1468.
(11) Werner, R. M.; Stivers, J. T. *Biochemistry* **2000**, *39*, 14054−14064.
(12) Chen, X.-Y.; Berti, P. J.; Schramm, V. L. *J. Am. Chem. Soc.* **2000**, *122*, 6527−6534.
(13) Birck, M. R.; Schramm, V. L. *J. Am. Chem. Soc.* **2004**, *126*, 6882−6883.
(14) Birck, M. R.; Schramm, V. L. *J. Am. Chem. Soc.* **2004**, *126*, 2447−2453.
(15) Stivers, J. T.; Jiang, Y. L. *Chem. Rev.* **2003**, *103*, 2729−2759.
(16) McCullough, A. K.; Dodson, M. L.; Lloyd, R. S. *Annu. Rev. Biochem.* **1999**, *68*, 255−285.
(17) Berti, P. J.; McCann, J. A. *Chem. Rev.* **2006**, *106*, 506−555.
(18) David, S. S.; Williams, S. D. *Chem. Rev.* **1998**, *98*, 1221−1261.
(19) Berti, P. J.; Tanaka, K. S. E. *Adv. Phys. Org. Chem.* **2002**, *37*, 239−314.
(20) Schramm, V. L. *Acc. Chem. Res.* **2003**, *36*, 588−596.

Scheme 1

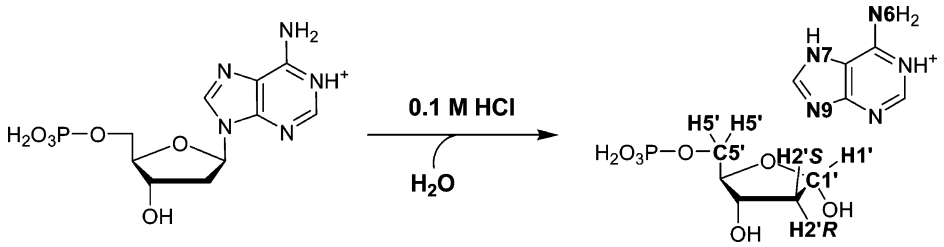

transition state. Weaker bonds at the transition state give normal KIEs, with the lighter atom reacting faster, $^{light}k/^{heavy}k > 1$. Stronger bonding gives inverse KIEs, $^{light}k/^{heavy}k < 1$. The reaction coordinate motion, i.e., leaving group departure and/or nucleophile approach, also contributes to the KIE. This makes it possible to distinguish between concerted (A_ND_N[21] or S_N2) and stepwise ($D_N{*}A_N$ or S_N1) mechanisms and to determine TS structures at subangstrom resolution in the best cases.[19] If the reaction is stepwise, it is also possible to distinguish reactions where the first step, leaving group departure, is irreversible ($D_N^{\ddagger}{*}A_N$)[22] from those where the C−N bond repeatedly breaks and reforms, followed by irreversible nucleophile attack ($D_N{*}A_N^{\ddagger}$).

Glycoside hydrolysis treads the borderline between stepwise and highly dissociative concerted transition states. TS analyses of uncatalyzed NAD^+ hydrolysis[2] and acid-catalyzed AMP hydrolysis[3,4,8] indicated highly dissociative A_ND_N mechanisms, though stepwise mechanisms could not be completely ruled out. A later QM/MM computational study of acid-catalyzed AMP hydrolysis yielded KIEs that were similar to the experimental values.[23] Leaving group departure is advanced over the nucleophile approach, resulting in a cationic, oxacarbenium ion-like ribosyl ring at the transition state. However, the 2′-hydroxy oxacarbenium ion is too unstable to form a discrete intermediate. The similar α-secondary ^{3}H KIEs for acid-catalyzed dAMP and AMP hydrolyses, 1.259 vs 1.253,[4,24] argued that dAMP would also proceed through an A_ND_N transition state. Studies on nonenzymatic hydrolyses of thymidine,[25] deoxyuridine,[25] deoxyadenosine (dAdo),[26] and dAMP[4] indicate oxacarbenium ion-*like* transition states but not necessarily a discrete oxacarbenium ion intermediate. Acid-catalyzed hydrolyses of 2-hydroxy- and 2-deoxyglycopyranosides have stepwise mechanisms with intermediate lifetimes on the order of 10^{-12}−10^{-10} s,[27−29] showing that oxacarbenium ion intermediates in water are possible.

TS analyses show that enzymatic reactions with ribosides generally have dissociative A_ND_N transition states,[3,6−8] though several stepwise reactions have been observed.[5,9,10] To date, TS analyses of enzymatic reactions with deoxyribosides have tended to the mechanistic extremes; thymidine phosphorylase formed an almost synchronous, noncationic A_ND_N transition state,[14] while uracil DNA glycosylase (UDG)[11] and ricin[12] catalyzed stepwise mechanisms.

We have used multiple KIE measurements on acid-catalyzed dAMP hydrolysis (Scheme 1) to determine the TS structure, in combination with determination of the anomeric product distribution.

Materials and Methods

General. ^{3}H- and ^{14}C-labeled glucoses were from American Radiolabeled Chemicals; ^{15}N-labeled compounds were from Cambridge Isotope Laboratories or Sigma-Aldrich. All other reagents and commercially available enzymes were from Sigma-Aldrich or Bioshop Canada (Burlington, ON). Liquiscint scintillation fluid (National Diagnostics) was used, except as noted. [6-^{15}N]-, [7-^{15}N]-, and [9-^{15}N]-adenines were synthesized by modification of literature procedures (see Supporting Information for details).[30] Bacterial strains overexpressing three of the enzymes for dATP synthesis were gifts and were purified or partially purified and assayed using modifications of literature procedures (see Supporting Information for details). They were phosphoribosyl pyrophosphate synthetase (PRPPase) from Bjarne Hove-Jensen (University of Copenhagen),[31] adenine phosphoribosyl transferase (APRTase) from Vern Schramm (Albert Einstein College of Medicine),[32] and ribonucleoside triphosphate reductase (RTRase) from JoAnne Stubbe (Massachusetts Institute of Technology).[33]

General dATP Synthesis. Labeled dAMPs were synthesized via ATP and dATP. The ATP synthesis method was modified from Parkin et al.[4] A solution containing 50 mM potassium phosphate, pH 7.6, 10 mM $MgCl_2$, 5 mM DTT, ≤1.1 mM labeled glucose, 0.1 mM ATP, 3.2 mM adenine, 20 mM PEP, and 5 mM NADP was prepared, and the pH was adjusted to ∼7.6 with 1 M KOH. MK (20 U/mL), 7 U/mL

(21) Mechanisms are described with IUPAC nomenclature. "A_N" represents nucleophilic association, and "D_N" represents nucleofugic dissociation. A concerted, bimolecular (S_N2) reaction is represented as A_ND_N. $D_N{*}A_N$ and $D_N + A_N$ mechanisms are stepwise (S_N1), with a discrete intermediate formed between leaving group departure and nucleophile approach. The signs "*" and "+" denote, respectively, an intermediate too short-lived for the leaving group to diffuse into solution and one that is diffusionally equilibrated with solvent. "P" indicates diffusional separation of the intermediate complex and is not normally written, unless it becomes kinetically significant. For stepwise mechanisms "‡" indicates the kinetically significant transition state, if known. Guthrie, R. D.; Jencks, W. P. *Acc. Chem. Res.* **1989**, *22*, 343−349.

(22) For KIEs measured by the competitive method, as in this study, the kinetically significant step is the *first irreversible step* rather than the rate-limiting step (see refs 12, 19, and Berti, P. J. *Methods Enzymol.* **1999**, *308*, 355−397). The degree of irreversibility of a given step is determined by the partitioning of the product of that step. Thus, in Scheme 3, the reversibility of oxacarbenium ion formation is given by k_5/k_4 (see eq 2).

(23) Barnes, J. A.; Williams, I. H. *Chem. Commun.* **1996**, 193−194.

(24) KIEs from other studies were converted to the same isotope and temperature as those used in this study. Other isotopes were converted using the Swain−Schaad relationship: ^{14}C-KIE = ^{13}C-KIE$^{1.89}$ and ^{3}H-KIE = ^{2}H-KIE$^{1.44}$. Other temperatures, T, were converted to 30 °C using $KIE_{303K} = \exp[\ln(KIE_T)\times(T/303)]$. (a) Swain, C. G.; Stivers, E. C.; Reuwer, J. F., Jr.; Schaad, L. J. *J. Am. Chem. Soc.* **1958**, *80*, 5885−5893. (b) Hirschi, J.; Singleton, D. A. *J. Am. Chem. Soc.* **2005**, *127*, 3294−3295. (c) Stern, M. J.; Spindel, W.; Monse, E. U. *J. Chem. Phys.* **1968**, *48*, 2908−2919.

(25) Shapiro, R.; Danzig, M. *Biochemistry* **1972**, *11*, 23−29. Shapiro, R.; Kang, S. *Biochemistry* **1969**, *8*, 1806−1810.

(26) Zoltewicz, J. A.; Clark, D. F.; Sharpless, T. W.; Grahe, G. *J. Am. Chem. Soc.* **1970**, *92*, 1741−1749.

(27) Amyes, T. L.; Jencks, W. P. *J. Am. Chem. Soc.* **1989**, *111*, 7888−7900. Zhu, J.; Bennet, A. J. *J. Am. Chem. Soc.* **1998**, *120*, 3887−3893. Lee, J. K.; Bain, A. D.; Berti, P. J. *J. Am. Chem. Soc.* **2004**, *126*, 3769−3776. Huang, X.; Surry, C.; Hiebert, T.; Bennet, A. J. *J. Am. Chem. Soc.* **1995**, *117*, 10614−10621. Bennet, A. J.; Kitos, T. E. *J. Chem. Soc., Perkin Trans. 2* **2002**, 1207−1222. Indurugalla, D.; Bennet, A. J. *J. Am. Chem. Soc.* **2001**, *123*, 10889−10898.

(28) Horenstein, B. A.; Bruner, M. *J. Am. Chem. Soc.* **1998**, *120*, 1357−1362.

(29) Zhu, J.; Bennet, A. J. *J. Org. Chem.* **2000**, *65*, 4423−4430.

(30) Pagano, A. R.; Lajewski, W. M.; Jones, R. A. *J. Am. Chem. Soc.* **1995**, *117*, 11669−11672. Orji, C. C.; Kelly, J.; Ashburn, D. A.; Silks, L. A., III. *J. Chem. Soc., Perkin Trans. 1* **1996**, 595−597.

(31) Hove-Jensen, B.; Harlow, K. W.; King, C. J.; Switzer, R. L. *J. Biol. Chem.* **1986**, *261*, 6765−6771.

(32) Shi, W. X.; Tanaka, K. S. E.; Crother, T. R.; Taylor, M. W.; Almo, S. C.; Schramm, V. L. *Biochemistry* **2001**, *40*, 10800−10809.

(33) Booker, S.; Stubbe, J. *Proc. Natl. Acad. Sci. U.S.A.* **1993**, *90*, 8352−8356.

glucose-6-phosphate dehydrogenase, 1 U/mL 6-phosphogluconate dehydrogenase, ~5 U/mL phosphoriboisomerase, 25 U/mL PK, 1 U/mL PRPPase, 0.75 U/mL APRTase, and 2 U/mL hexokinase were added, and the reaction was incubated at 37 °C for 2 h. ^{3}H syntheses contained 25 μCi in 22 μL, while ^{14}C syntheses contained 10 μCi in 182 μL. No carrier (unlabeled) glucose was added.

Except for the 2′-^{2}H labels, the ATP reaction mixtures were taken directly to dATP. DTT (25 mM), 20 μM coenzyme B12, and 0.9 mg/mL RTRase were added after 2 h, and then the mixture was degassed with three cycles of vacuum for 30 s and flushing with N_2 gas. The reaction was incubated in the dark at 37 °C for 2 h. Protein was removed by centrifugal ultrafiltration (Microcon YM10, Millipore) at 14 000 × *g* and 4 °C. dATP was purified from the filtrate by C18 reversed phase HPLC (Waters, 4.6 mm × 250 mm, 15 μm particle) with 97% 50 mM triethylammonium acetate (TEAA, pH 6.0) and 3% MeOH at 2 mL/min. Fractions containing dATP were lyophilized repeatedly to remove residual salts and stored at −80 °C.

[2′-*S*-^{2}H,5′-^{14}C]- and [2′-*R*-^{2}H,5′-^{14}C]dATP. [2′*S*-^{2}H,5′-^{14}C]dATP was synthesized by a modification of the method of Werner and Stivers.[11] Reagents were prepared in 99.9% D_2O, with repeated lyophilization. The pD was adjusted to ~7.6 with 10 M of 99.5% NaOD. The enzymes were combined with 50 mM potassium phosphate, pD 7.6, in D_2O, and the buffer was exchanged by ultrafiltration. [2′*S*-^{2}H,5′-^{14}C]ATP was purified as described above for dATP. It was then reduced in H_2O to dATP as described above and purified. [2′*R*-^{2}H,5′-^{14}C]dATP was made from [5′-^{14}C]ATP which had been synthesized and purified as above. Reduction to dATP in D_2O gave 2′*R*-^{2}H incorporation. The dADP peak in negative ion mass spectra (m/z_{calcd} = 410.0, unlabeled) was ~10-fold stronger than that of dATP (m/z_{calcd} = 490.0, unlabeled) and was used to determine isotopic enrichment. MS (ESI-) *m*/*z* (intensity): [2′*S*-^{2}H,5′-^{14}C]dADP: m/z_{calcd} = 413.0; m/z_{obsd} = 411.1 (35%), 412.1 (13%), and 413.1 (100%). Of ^{14}C-containing dATP, 96% was [2′*S*-^{2}H,5′-^{14}C]dATP.[34] [2′*R*-^{2}H,5′-^{14}C]dADP: m/z_{calcd} = 413.0; m/z_{obsd} = 411.1 (58%), 412.1, (13%), and 413.1 (100%). Of ^{14}C-containing dATP, 95% was [2′*R*-^{2}H,5′-^{14}C]dATP. The experimental KIEs were corrected for the extent of labeling.

General dAMP Synthesis. Reaction mixtures containing ≤1 mM of ^{3}H- or ^{14}C-labeled dATPs (1.4 × 10^6 counts per min, cpm), 2 mM unlabeled ATP, 6.25 mM glucose, 10 mM $MgCl_2$, 25 U/mL hexokinase, 200 U/mL myokinase, and 50 mM potassium phosphate, pH 7.6 were incubated at 37 °C for 2 h. dAMP was purified similarly to the purification for the dATP synthesis, except using 98.5% 50 mM TEAA, pH 6.0, and 1.5% MeOH. The chemical concentration of [^{14}C]dAMPs was determined using ϵ_{260} = 15.1 mM^{-1} cm^{-1}.[35] The chemical concentration of ^{3}H-labeled dAMP was negligible given its high specific activity and was not measured.

dAMP Solvolysis Kinetics. dAMP hydrolysis rates were measured with 1.25 mM dAMP in 0.1 M HCl at 30 °C. Reaction aliquots (10−100 μL) were neutralized with a 40 μL 1 M potassium phosphate, pH 6.0, diluted to 200 μL with water, and analyzed by C18 reversed phase HPLC chromatography (25 cm × 4.6 mm, Supelcosil LC-18-T, 5 μm particles) at 1 mL/min using 40:60 A/B (solvent A = 20% MeOH, 80% 100 mM potassium phosphate, pH 7.2, 4 mM TBAS; solvent B = 100 mM potassium phosphate, pH 6.0, 4 mM TBAS) with A_{260} detection. Fractional extents of reaction were determined from the dAMP peak area at each time point relative to the initial dAMP area. Aliquot volumes were increased as the reaction progressed to maintain reasonable dAMP peak sizes. The rate constants for dAMP breakdown were determined by nonlinear least-squares fits to the first-order rate equation. Rates measured using [5′-^{14}C]dAMP and scintillation counting gave identical results.

Scheme 2

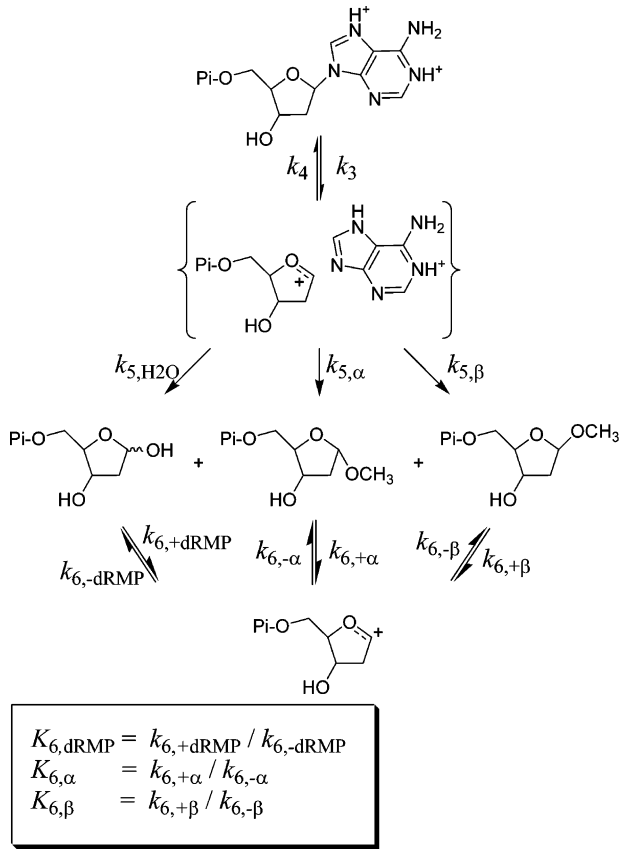

dRMP and α-/*β*-Me-dRMP. [5′-^{14}C]dRMP was synthesized by incubating 1.25 mM [5′-^{14}C]dAMP (10^6 cpm) in 0.1 M HCl for 24 h at 30 °C and was used without purification. Anomerically pure [5′-^{14}C]α-Me-dRMP and [5′-^{14}C]*β*-Me-dRMP were synthesized by incubating 1.25 mM [5′-^{14}C]dAMP (10^6 cpm) in MeOH/0.1 M HCl at 30 °C for 48 h, followed by purification by C18 reversed-phase HPLC (Waters Delta Pak C18, 7.8 mm × 300 mm, 15 μm particles) using 50 mM TEAA, pH 6.0, at 4 mL/min. α- and *β*-Me-dRMP eluted at 6.7 and 8.8 min, respectively, and were lyophilized repeatedly. Their identities were confirmed by comparison with unlabeled α- and *β*-Me-dRMP (see Supporting Information).

dRMP and α-/*β*-Me-dRMP Kinetics. Solvolysis reactions were followed by adding 50% MeOH/0.1 M HCl to 5′-^{14}C-labeled dRMP, α-Me-dRMP, or *β*-Me-dRMP and analyzing 30 000 cpm aliquots by HPLC as in the case for dAMP solvolysis, except with solvents 25:75 A/B and inline flow scintillation analysis to detect ^{14}C, with 4 mL/min Ultima-Flo M scintillation fluid (Packard) mixed with the eluate.

Rate constants, $k_{6,\pm n}$, and equilibrium constants, $K_{6,n}$, were determined by numerical simulation of the kinetic mechanism (Scheme 2) using KinTekSim,[36] an implementation of FitSim[37] and KinSim.[38] The $k_{6,+n}$ rate constants were on the order of 10^{-4} to 10^{-3} s^{-1} and were well determined by the experimental data. The values of $k_{6,-n}$ are on the order of 10^{11} s^{-1} and cannot be determined from the experimental data beyond stating that they are much larger than $k_{6,+n}$. Because the numerical simulation software could not handle the 10^{14}-fold range between $k_{6,+n}$ and $k_{6,-n}$, initial values of $k_{6,-n}$ were set to an arbitrarily

(34) *m*/*z* = 411 corresponds to [2′*S*-^{2}H]dATP. This arises because the ^{14}C-labeled glucose contains an unlabeled carrier. It is not radioactive and, therefore, not visible by scintillation counting. *m*/*z* = 412 corresponds to [5′-^{14}C]-dADP, plus natural abundance isotopes (mostly ^{13}C) adding 1 to the *m*/*z* = 411 peak. The relative intensities in unlabeled dATP was I_{411}/I_{412} = 1:0.21. Subtracting the contribution from natural abundance isotopes to the *m*/*z* = 412 peak, the ratio I_{412}/I_{413} was 4:96. Thus, 96% of ^{14}C-labeled dATP contained ^{2}H, i.e., was [2′*S*-^{2}H, 5′-^{14}C]dATP.

(35) *Short Protocols in Molecular Biology*; Ausubel, F. M., Smith, J. A., Moore, D. D., Brent, R., Seidman, J. G., Struhl, K., Kingston, R. E., Eds.; Wiley: New York, 1999.

(36) Dang, Q.; Frieden, C. *Trends Biochem. Sci.* **1997**, *22*, 317.

(37) Zimmerle, C. T.; Frieden, C. *Biochem. J.* **1989**, *258*, 381−387.

(38) Barshop, B. A.; Wrenn, R. F.; Frieden, C. *Anal. Biochem.* **1983**, *130*, 134−145.

Table 1. Kinetic Constants and Equilibrium Percentages for dRMP, α-Me-dRMP, and β-Me-dRMP Solvolysis in 50% MeOH/0.1 M HCl at 30 °C[a]

	dRMP	α-Me-dRMP	β-Me-dRMP
$k_{6,+n}$[b]	1.7 (±0.8) × 10^{-3} s^{-1}	2.23 (±0.002) × 10^{-4} s^{-1}	2.7 (±0.3) × 10^{-4} s^{-1}
$K_{6,n}$(relative)[c]	3.3 ± 0.3	1	1.2 ± 0.1
equilibrium percentages[d]	14 ± 1	47 ± 1	39 ± 1

[a] Two independent replicates were run with each starting material: dRMP and α-/β-Me-dRMP. The means of constants from all three starting materials are reported. [b] $k_{6,+n}$ is $k_{6,+dRMP}$, $k_{6,+\alpha}$, or $k_{6,+\beta}$. [c] $K_{6,n}$(relative) = $K_{6,n}/K_{6,\alpha}$, and $K_{6,n} = k_{6,+n}/k_{6,-n}$. [d] Final product concentrations after 300 min.

large number, 10^5 s^{-1}, and then optimized. The absolute values of $k_{6,+n}$ (see Table S3) had no significance beyond being $\gg k_{6,-n}$. Their relative values were well-determined, though, and used to calculate $K_{6,n}$ (relative) (see Table 1).

dAMP Solvolysis in 50% MeOH. [5′-^{14}C]dAMP (1.25 mM, 10^6 cpm) was incubated in 50% MeOH/0.1 M HCl for 3 min at 30 °C. Aliquots were neutralized and analyzed by HPLC as in the case for dAMP hydrolysis, except with solvents 25:75 A/B, with 1 mL fractions collected, mixed with 10 mL of scintillation fluid, and counted for 5 × 10 min. Rate and equilibrium constants were fitted to the kinetic mechanism (Scheme 2) by numerical simulation.

Kinetic Isotope Effect Measurements. Competitive KIEs were measured by making a mixture of the isotopic label of interest and a remote label (e.g., 1′-^{3}H and 5′-^{14}C, respectively) and measuring the ^{3}H/^{14}C ratio in the products of partial reactions compared with reactions taken to completion.[39] For ^{15}N KIEs, 5′-^{14}C was used as a reporter on ^{15}N, and 5′,5′-$^3H_2$ was the remote label. dAMP (1.25 mM, 180 000 cpm each of ^{3}H and ^{14}C, in 300 μL) was incubated in 0.1 M HCl at 30 °C for 90 min (∼$t_{1/2}$). A 200 μL aliquot was diluted with 1300 μL of elution buffer (100 mM potassium phosphate, pH 6.0, 100 mM ribose, and 10% EtOH), from which 100 μL were used to determine the extent of reaction (see below). The remaining 100 μL of reaction mixture were reacted for >19 h (>13 × $t_{1/2}$), and 1400 μL of elution buffer were added. Adenine and residual dAMP were separated from dRMP using charcoal columns.[14] Acid-washed activated charcoal[4] (190 mg/mL) was suspended in elution buffer; 525 μL were applied to Qiagen or Sigma mini-prep spin columns, packed by centrifugation at 400 × *g* for 1 min in a swinging bucket rotor, and then washed with 3 × 500 μL of elution buffer. Three 500 μL aliquots of the reaction mixtures were purified on individual charcoal columns using centrifugation as above, with dRMP eluted in 5 × 500 μL of elution buffer. The eluate, 3 mL total, was collected directly into a 24 mL plastic scintillation vial, and the liquid weight in each scintillation vial was equalized with elution buffer before adding 19 mL of scintillation fluid. The ^{3}H/^{14}C ratios were measured by counting samples in 10 min cycles using dual channel scintillation analysis, until ≥360 000 counts were collected in the ^{14}C channel.[39] KIEs were calculated using eq 1,[40]

$$\mathrm{KIE} = 1 + \frac{\ln\left(1 + \left(\frac{A/A' - X/X'}{A/A'}\right)\left(\frac{f\left(\frac{1 + A/A'}{1 + X/X'}\right)}{1 - f\left(\frac{1 + A/A'}{1 + X/X'}\right)}\right)\right)}{\ln\left(1 - f\left(\frac{1 + A/A'}{1 + X/X'}\right)\right)} \quad (1)$$

where radioactive counts in the complete reaction are *A* for the remote label and *A*′ for the label of interest. In the partial reaction, they are *X* for the remote label and *X*′ for the label of interest. The fractional extent of reaction, *f*, was determined by separating the reactants and products by reversed phase HPLC as in the case for dAMP kinetics but with solvents 60:40 A/B. Fractions (14 × 1 mL) were mixed with 10 mL of scintillation fluid, and radioactivity was counted for 10 min to determine product (fractions 4 and 5) and residual substrate (fractions 9−13).

Scheme 3

$$\mathrm{dAMP^{N1H}} \underset{k_2}{\overset{k_1}{\rightleftharpoons}} \mathrm{dAMP^{N1H}_{N7H}} \underset{k_4}{\overset{k_3}{\rightleftharpoons}} \{\mathrm{oxac{\cdot}\ adenine}\} \xrightarrow{k_5} \mathrm{dRMP + adenine^{N1H}_{N7H}}$$

Quantum Mechanical Calculations. Quantum mechanical calculations were performed using hybrid density functional theory (DFT) with Becke's exchange functional,[41] Perdew and Wang's correlation functional,[42] and a 6-31+G** basis set (B3PW91/6-31+G**) with Gaussian 98.[43] Optimized structures had no imaginary frequencies, and transition states had one. Intrinsic reaction coordinate calculations[44] showed the expected nucleophile and/or leaving group motions along the reaction coordinate.

EIE and KIE Calculation. Quiver[45] was used to calculate reduced isotopic partition functions (*Q*) at 303 K. The Cartesian force constants were scaled by 0.9139 (=0.956^2).[46] Equilibrium isotope effects (EIEs) were calculated as EIE = $Q_{initial}/Q_{final}$.

For transition states, KIE = $Q_{initial}/Q^{\ddagger}$ × $^{light}\upsilon^*/^{heavy}\upsilon^*$, where $^{light}\upsilon^*/^{heavy}\upsilon^*$ is the Teller−Redlich product ratio in the Quiver output. Stepwise $D_N{}^*A_N$ reactions have two transition states, and the observable KIEs are a function of partitioning of the oxacarbenium ion intermediate in the forward (k_5) and reverse (k_4) directions (Scheme 3):[12]

$$\mathrm{KIE} = \frac{\frac{\alpha_1\alpha_3}{\alpha_2}\left(\frac{\alpha_5}{\alpha_4} + \frac{k_5}{k_4}\right)}{1 + \frac{k_5}{k_4}} \quad (2)$$

and α_n is the intrinsic KIE on step *n*, i.e., $\alpha_n = {}^{light}k_n/{}^{heavy}k_n$.

Results

Solvolysis Studies. When the experimental KIEs indicated a stepwise mechanism, methanolysis reactions were used to investigate the products' anomeric distribution and probe the oxacarbenium ion's lifetime.

The pseudo-first-order rate constant for dAMP hydrolysis was $k_{hydrolysis}[H^+] = 1.32\ (\pm 0.01) \times 10^{-4}\ s^{-1}$ in 0.1 M HCl (pH 1). This gives a second-order rate constant of $k_{hydrolysis} = 1.32 \times 10^{-3}\ M^{-1}\ s^{-1}$, *cf.*, the literature value, $1.25 \times 10^{-3}\ M^{-1}\ s^{-1}$.[47] The rate was $k_{solvolysis} = 5.3\ (\pm 0.2) \times 10^{-5}\ s^{-1}$ in 50% MeOH/0.1 M HCl. This modest change implies that the mechanism does not change in 50% MeOH and that the anomeric product distribution should accurately reflect the hydrolysis reaction.

(39) Parkin, D. W. In *Enzyme mechanism from isotope effects*; Cook, P. F., Ed.; CRC Press, Inc.: Boca Raton, FL, 1991; pp 269−290.
(40) Bigeleisen, J.; Wolfsberg, M. *Adv. Chem. Phys.* **1958**, *1*, 15−76.
(41) Becke, A. D. *Phys. Rev. A* **1988**, *38*, 3098−3100.
(42) Perdew, J. P.; Wang, Y. *Phys. Rev. B* **1992**, *45*, 13244.
(43) Frisch, M. J., et al. *Gaussian 98*; Gaussian, Inc.: Pittsburgh, PA, 1998.
(44) Gonzalez, C.; Schlegel, H. B. *J. Chem. Phys.* **1989**, *90*, 2154−2161. Gonzalez, C.; Schlegel, H. B. *J. Phys. Chem.* **1990**, *94*, 5523−5527.
(45) Saunders, M.; Laidig, K. E.; Wolfsberg, M. *J. Am. Chem. Soc.* **1989**, *111*, 8989−8994.
(46) Wong, M. W. *Chem. Phys. Lett.* **1996**, *256*, 391−399.
(47) Hakala, H.; Oivanen, M.; Saloniemi, E.; Gouzaev, A.; Lonnberg, H. *J. Phys. Org. Chem.* **1992**, *5*, 824−828.

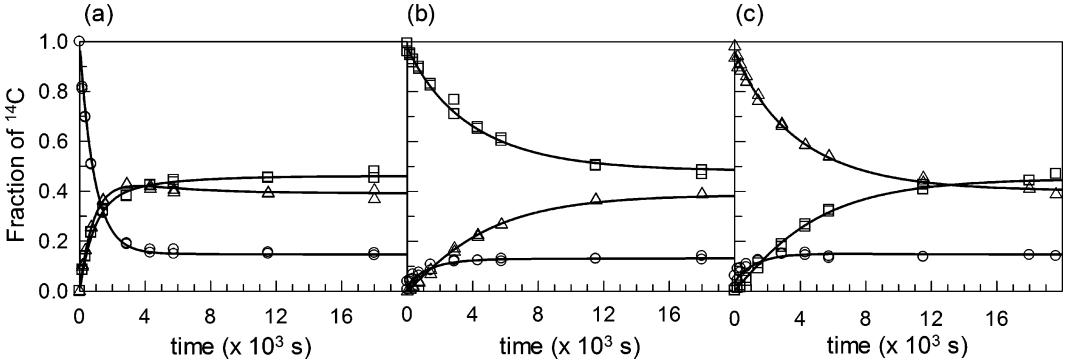

Figure 1. Time course of reactions in 50% MeOH/0.1 M HCl, 30 °C, starting from (a) [5′-^{14}C]dRMP, (b) [5′-^{14}C]α-Me-dRMP, or (c) [5′-^{14}C]β-Me-dRMP. (○) [5′-^{14}C]dRMP, (□) [5′-^{14}C]α-Me-dRMP, (△) [5′-^{14}C]β-Me-dRMP. The lines are from the fits to the kinetic mechanism to determine the rate constants $k_{6,\pm n}$ (Scheme 2, Table 1).

Table 2. Products of dAMP Solvolysis in 50% MeOH/0.1 M at 30 °C for 3 min[a]

species	dRMP	α-Me-dRMP	β-Me-dRMP
% (observed)[b]	59 ± 1	36 ± 1	6 ± 1
% (corrected)[c]	61	34	4
α/β ratio (corrected)		8.5	1

[a] Average of two experiments. [b] Standard error for five cycles of scintillation counting, 10 min per cycle. [c] Corrected using Scheme 2 and the individual estimates of $K_{6,dRMP}$, $K_{6,\alpha}$, and $K_{6,\beta}$ determined from each plot in Figure 1.

Reactions in 50% MeOH/0.1 M HCl produced dRMP, α-Me-dRMP, and β-Me-dRMP (Scheme 2). These products are more acid labile than dAMP, so reactions to determine the products' anomeric distribution were limited to 3 min (<1% reaction) and were corrected for interconversion. Interconversion rates were determined by reacting dRMP, α-, and β-Me-dRMP under the same conditions and fitting the reaction profiles by numerical simulation (Figure 1, Tables 1, S3). This showed that, in dAMP reactions at $t = 3$ min, one-third of the β-Me-dRMP had arisen from dRMP and α-Me-dRMP solvolysis (Table 2). These rate constants gave a nucleophile selectivity, $k_{MeOH}/k_{H_2O} = 1.40 \pm 0.01$.[29,48,49]

β-Me-dRMP arising directly from dAMP can only form after dissociation of the contact ion pair complex (CIPC), {**2**•N1H,-N7H-**5**}, to a solvent-separated ion pair complex (SSIPC) or complete dissociation to free **2** (Scheme 4). Methanol will be occluded from the β-face in a CIPC. The ratio of α-Me-dRMP/β-Me-dRMP arising directly from dAMP was 8.5:1. Assuming that **2** is equally susceptible to attack on either face after CIPC dissociation, the amount of α-Me-dRMP arising after CIPC dissociation would equal β-Me-dRMP. Acid-catalyzed solvolysis of CMP-NeuAc in aqueous methanol proceeds through an oxacarbenium ion intermediate and yields 1:1 α-/β-methyl NeuAc,[28,50] demonstrating that its oxacarbenium ion (**9**) is equally susceptible to attack on either face. Thus, the ratio of products from the CIPC (α-Me-dRMP only) to the dissociated oxacarbenium ion (α- and β-Me-dRMP) would be 7.5:2 or approximately 80% vs 20%.

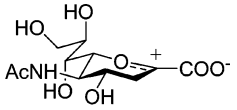

9

Experimental KIEs. KIEs were measured using the competitive method (Table 3). The 1′-^{3}H KIE was reported previously at 1.259 ± 0.006,[4] within experimental error of the value of 1.253 ± 0.002 found in this study. Note that the 95% confidence interval is reported in the present study, rather than the standard error reported for the literature value.

Computational Structures. Gas-phase structural optimizations are not necessarily accurate models of solution-phase reactions. In this study, the agreement of calculated with experimental IEs lent support to the computational models (see Discussion). The reactant species, N1H-dAMP, was modeled with N1H-**1** and N1H-**3** (Figure 2). In 0.1 M HCl, dAMP is 94% monoprotonated at N1, 5% at N7, with ≤0.5% each of the unprotonated and diprotonated forms.[51] Correcting for the minor forms would change the 7-^{15}N KIE by <0.001. Compounds **1** and **3** reflected the dominant solution conformations, based on X-ray,[52] NMR,[53] molecular dynamics,[54] and *ab initio*[55,56] structures. They were *gauche*−*gauche* (g^+,g^+) about the C4′−C5′ and C5′−O5′ bonds, with an *anti* adenine base and a 2′-*endo* deoxyribosyl ring conformation.[57] Minor conformers will exist, but the small energy differences and small barriers to interconversion mean that they will have negligible effects on the IEs.[56,58] The 2-deoxyoxacarbenium ion (**2**)

(48) nucleophile selectivity = k_{MeOH}/k_{H_2O} = (([α − Me − dRMP] + [β − Me − dRMP])[H_2O])/[dRMP][MeOH]. (a) Tashma, R.; Rappoport, Z. *Adv. Phys. Org. Chem.* **1992**, *27*, 239−291.
(49) Knoll, T. L.; Bennet, A. J. *J. Phys. Org. Chem.* **2004**, *17*, 478−482.
(50) Horenstein, B. A.; Bruner, M. *J. Am. Chem. Soc.* **1996**, *118*, 10371−10379.
(51) Given p$K_{a,N1}$ = 3.7, a microscopic p$K_{a,N7}$ ≈ 2.4, and a macroscopic p$K_{a,N1H,N7H}$ = −1.3 for diprotonation. (a) Remaud, G.; Zhou, X. X.; Chattopadhyaya, J.; Oivanen, M.; Lonnberg, H. *Tetrahedron* **1987**, *43*, 4453−4461. (b) Acharya, P.; Cheruku, P.; Chatterjee, S.; Acharya, S.; Chattopadhyaya, J. *J. Am. Chem. Soc.* **2004**, *126*, 2862−2869. (c) Kampf, G.; Kapinos, L. E.; Griesser, R.; Lippert, B.; Sigel, H. *J. Chem. Soc., Perkin Trans. 2* **2002**, 1320−1327.
(52) Gelbin, A.; Schneider, B.; Clowney, L.; Hsieh, S. H.; Olson, W. K.; Berman, H. M. *J. Am. Chem. Soc.* **1996**, *118*, 519−529.
(53) Bandyopadhyay, T.; Wu, J.; Serianni, A. S. *J. Org. Chem.* **1993**, *58*, 5513−5517. Bandyopadhyay, T.; Wu, J.; Stripe, W. A.; Carmichael, I.; Serianni, A. S. *J. Am. Chem. Soc.* **1997**, *119*, 1737−1744. Altona, C.; Sundaralingam, M. *J. Am. Chem. Soc.* **1972**, *94*, 8205−8211. Altona, C.; Sundaralingam, M. *J. Am. Chem. Soc.* **1973**, *95*, 2333−2344. Davies, D. B.; Danyluk, S. S. *Biochemistry* **1974**, *13*, 4417−4434.
(54) Foloppe, N.; Nilsson, L. *J. Phys. Chem. B* **2005**, *109*, 9119−9131.
(55) Shishkin, O. V.; Gorb, L.; Zhikol, O. A.; Leszczynski, J. *J. Biomol. Struct. Dyn.* **2004**, *22*, 227−243. Foloppe, N.; MacKerell, A. D. *J. Phys. Chem. B* **1998**, *102*, 6669−6678.
(56) Foloppe, N.; Hartmann, B.; Nilsson, L.; MacKerell, A. D. *Biophys. J.* **2002**, *82*, 1554−1569.
(57) Furanosyl ring puckers are indicated with n-*endo* and n-*exo* designations, where all ring atoms except n are in the same plane. Atom n is displaced toward the 5′-substituent in n-*endo* conformers and away in n-*exo*. (a) Joint Commission on Biochemical Nomenclature. *Pure Appl. Chem.* **1983**, *55*, 1273−1280.

Scheme 4

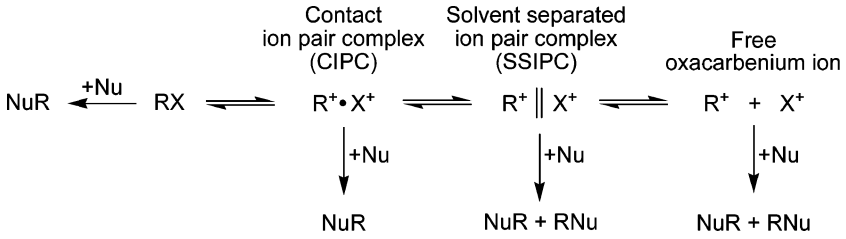

Table 3. KIEs for Acid-Catalyzed dAMP Hydrolysis

isotope of interest[a]	type of KIE	experimental KIE[b]
1′-^{14}C	primary ^{14}C	1.004 ± 0.002 (3)
9-^{15}N	primary ^{15}N	1.022 ± 0.003 (4)
6-^{15}N	secondary ^{15}N	0.997 ± 0.006 (6)
7-^{15}N	secondary ^{15}N	0.985 ± 0.002 (3)
1′-^{3}H	α-secondary ^{3}H	1.253 ± 0.002 (3)
2′*S*-^{2}H	*β*-secondary ^{2}H	1.113 ± 0.007 (5)
2′*R*-^{2}H	*β*-secondary ^{2}H	1.091 ± 0.002 (3)
5′,5′-$^{3}H_2$[c]	*δ*-secondary ^{3}H	1.012 ± 0.002 (3)

[a] 1′-^{3}H and 5′,5′-$^{3}H_2$ KIEs were measured using a mixture of the ^{3}H and [5′-^{14}C]dAMPs. 5′-^{14}C was the remote label and was assumed to have a KIE of unity. The 1′-^{14}C KIE was determined with 5′,5′-$^{3}H_2$ as the remote label and was corrected for the 5′,5′-$^{3}H_2$ KIE. ^{2}H and ^{15}N KIEs were measured by incorporating 5′-^{14}C as a reporter radionuclide (e.g., [9-^{15}N,5′-^{14}C]dAMP), with 5′,5′-$^{3}H_2$ as the remote label. [b] Errors are the 95% confidence intervals. The number of independent KIE measurements is in parentheses. KIEs were corrected for the presence of incomplete labeling with nonradioactive labels, i.e., 3% [9-^{14}N,5′-^{14}C], 2% [6-^{14}N,5′-^{14}C], 4% [2′*S*-^{1}H,5′-^{14}C], or 5% [2′*R*-^{1}H,5′-^{14}C].[39] [c] [5′,5′-$^{3}H_2$] was doubly labeled at the 5′ position. Experimental and calculated KIEs are reported for the doubly labeled material, not per ^{3}H. ^{3}H was used in trace amounts, so the molar fraction of ^{3}H-labeled dAMP was negligible.

optimized as the 3′-*exo* conformer. Attempts to optimize a 3′-*endo* conformer resulted in it reverting to 3′-*exo*.

Computational transition states were found for A_ND_N (N1H,N7H-**6**‡), $D_N{}^{‡}{*}A_N$ (N1H,N7H-**7**‡), and $D_N{*}A_N{}^{‡}$ (α-**8a**‡, α-**8b**‡) mechanisms. α-**8a**‡ and α-**8b**‡ had the water nucleophile in different locations, consistent with the small intrinsic barrier to nucleophilic attack on oxacarbenium ions,[59] and with multiple local saddle points (Figure 3). The bond length and angle of nucleophile approach in α-**8a**‡ were similar to those of previously reported structures using simpler oxacarbenium ion models.[12] The C1′−O bond length in α-**8b**‡ was considerably shorter. The reaction coordinate motion (the normal mode with an imaginary frequency) corresponded largely to a rotation of the water molecule. At long distances, the H_2O−**2** interaction is primarily electrostatic and H_2O approaches **2** with the most negative electrostatic potential oriented toward C1′. Rotation of H_2O (with the protons moving out of the plane of page in Figure 3, toward the reader) allows oxygen to rehybridize and form electron lone pairs and form a covalent bond with C1′. A transition state for *β*-attack, *β*-**8**‡, was also found (see Supporting Information). Intermediates **2**, **4**, and N1H,N7H-**5** were used to calculate KIEs for a $D_N{*}P^{‡}{+}A_N$ mechanism (see below). Compounds **1** and N7H-**7**‡ showed the effect of N1 protonation on the transition state.

Calculated KIEs and EIEs. KIEs and EIEs were calculated from the computationally optimized models (Figure 2, Table 4). The 5′-phosphate group was removed from the TS models to simplify the calculations. This is justified by its <2-fold effect on hydrolysis rates[47] and a small effect on the reactant's electrostatic potential surface (see Figure 5). This caused changes of ≤0.009 in the calculated 1′-^{3}H and 2′-^{2}H EIEs and no changes in the heavy atom EIEs (Table 4). There was a large effect on the calculated 5′,5′-$^{3}H_2$ EIE for oxacarbenium ion formation, 1.038 with 5′-phosphate vs 1.007 without.

Discussion

KIEs and Mechanism. TS analysis demonstrated a stepwise mechanism with reversible C−N bond cleavage followed by either (*i*) irreversible water attack on the oxacarbenium ion in the CIPC ~80% of the time or (*ii*) irreversible dissociation of the CIPC ~20% of the time (Table 4).[60] Thus, the mechanism of dAMP hydrolysis is 80% $D_N{*}A_N{}^{‡}$/20% $D_N{*}P^{‡}{+}A_N$. The calculated heavy atom KIEs, 1′-^{14}C, 9-^{15}N, and 7-^{15}N, were within 0.002 of the experimental values for the α-**8a**‡ transition state, with a difference of 0.003 for 1′-^{14}C with the α-**8b**‡ transition state. Previously it was only possible to distinguish between stepwise and concerted mechanisms, but with more complete computational models it is now possible to distinguish between different stepwise mechanisms (see below).

The best match of calculated to experimental hydron (^{2}H and ^{3}H) KIEs was with this mechanism, although, as observed previously, the match of calculated to experimental KIEs was not as close as that for the heavy atom KIEs. This trend has been observed previously, where the calculated hydron KIEs do not match the experimental values as well as the heavy atom KIEs.[5,9,10,12,61] The experimental hydron KIEs matched well with related reactions (see below).

Observable KIEs. Competitive KIEs report on the *first irreversible* transition state of the reaction (or more than one step if there are partially irreversible steps before the first fully irreversible one).[19] There are at least two transition states for a stepwise mechanism: leaving group departure, the D_N step, and nucleophile attack, A_N. The observable KIEs depend on partitioning of the oxacarbenium ion intermediate (eq 2, Scheme 3).[12] If $k_5 \gg k_4$ then the D_N step is irreversible and KIEs reflect $D_N{}^{‡}$ only. This is a $D_N{}^{‡}{*}A_N$ mechanism or $D_N{}^{‡}$ + A_N if the intermediates exist long enough for the CIPC to dissociate. The 1′-^{14}C KIE for the D_N step was 1.052, much higher than the experimental value. If $k_5 \ll k_4$, then the D_N step is reversible, and **1** is in equilibrium with {**2**•N1H,N7H-**5**}. The first irreversible step is either (*i*) water attack to form **8**‡, the $A_N{}^{‡}$ step of a $D_N{*}A_N{}^{‡}$ mechanism, or (*ii*) dissociation of the CIPC, giving a $D_N{*}P^{‡}{+}A_N$ mechanism ("P" indicates diffusional separation and is not generally written unless it is kinetically

(58) Gabb, H. A.; Harvey, S. C. *J. Am. Chem. Soc.* **1993**, *115*, 4218−4227. Arora, K.; Schlick, T. *Chem. Phys. Lett.* **2003**, *378*, 1−8.
(59) Richard, J. P. *Tetrahedron* **1995**, *51*, 1535−1573. Richard, J. P.; Williams, K. B.; Amyes, T. L. *J. Am. Chem. Soc.* **1999**, *121*, 8403−8404.
(60) *β*-Me-dRMP could arise from either a $D_N{}^{‡}{*}P{+}A_N$ or $D_N{*}P^{‡}{+}A_N$ mechanism. However, assuming a 20% contribution from a $D_N{}^{‡}{*}P{+}A_N$ mechanism gives an observable 1′-^{14}C KIE of 1.013−1.017, outside the error range of the experimental value.
(61) Singh, V.; Schramm, V. L. *J. Am. Chem. Soc.* **2006**, *128*, 14691−14696.

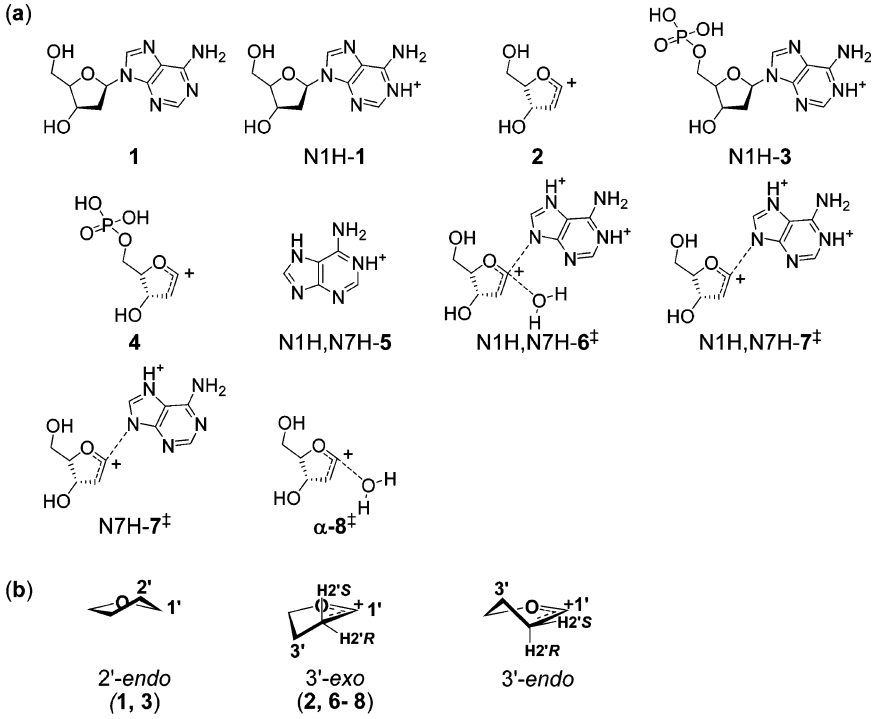

Figure 2. (a) Reactant (**1**, N1H-**1**, and N1H-**3**), intermediate (**2**, **4**, and N1H,N7H-**5**), and TS (N1H,N7H-**6**‡, N1H,N7H-**7**‡, N7H-**7**‡, α-**8**‡) models used to calculate IEs. (b) Sugar ring conformers.

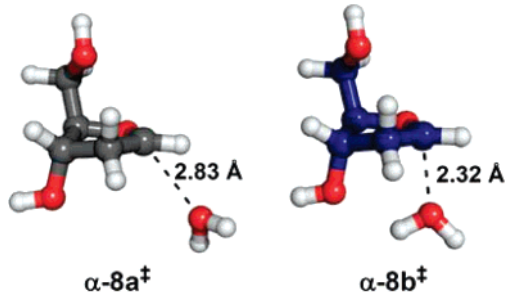

Figure 3. TS models α-**8a**‡ and α-**8b**‡ of water attack on **2**.

significant). KIEs on dissociation should be small, so the observable KIEs for a $D_N{*}P^{\ddagger}{+}A_N$ mechanism will equal the EIEs of C−N bond cleavage. At intermediate values of k_5/k_4, the observable KIEs vary monotonically between the extremes.

Reliability of Calculated KIEs. The accuracy of the calculated IEs depends on the accuracy of the computational models. It was limited in this study by how well the gas-phase calculations reflected the geometries and structures of solution-phase reactions. Gas-phase calculations are often not accurate models of solution-phase reactions. However, several studies have established that the frequencies calculated by post-Hartree−Fock methods, including hybrid DFT, accurately reflect molecular structure[46,62] and therefore that calculated IEs also accurately reflect those structures whether or not those structures accurately reflect reality. If the calculated KIEs match the experimental values, that is good evidence that the calculated structures match the true structures. If the calculated KIEs do not match the experimental ones, then the calculated structures are incorrect and it would be necessary to use bond order vibrational analysis to interpret the KIEs.[63] In this study, the calculated KIEs did match the experimental KIEs, which indicates that the calculated structures accurately reflect the solution-phase reactions.

Primary 1′-^{14}C KIE. The calculated 1′-^{14}C KIEs for a $D_N{*}A_N^{\ddagger}$ mechanism were an excellent match when the 20% $D_N{*}P^{\ddagger}{+}A_N$ mechanism was included. The experimental value, 1.004, was in the range observed previously for stepwise purine nucleoside reactions, 0.993−1.015.[5,9,10,12] Experimental 1′-^{14}C KIEs from reactions with A_ND_N transition states range from 1.020 for highly dissociative[2,24] to 1.139 for almost synchronous[13] transition states. The calculated A_ND_N KIE, 1.059, fits in this range. The calculated $D_N^{\ddagger}{*}A_N$ 1′-^{14}C KIE was higher than previously expected for a stepwise mechanism (see below).

^{15}N KIEs and Leaving Group Protonation. All the calculated 9-^{15}N KIEs were excellent matches for the experimental 9-^{15}N KIE. The 9-^{15}N KIE indicated significant or complete C1′−N9 bond cleavage at the transition state but did not distinguish between mechanisms.

The calculated 7-^{15}N KIE for a $D_N{*}A_N^{\ddagger}$ mechanism, 0.987, agreed well with the experimental value, 0.985. Protonation creates a more vibrationally constrained environment for the protonated atom and therefore an inverse KIE. The KIE indicated that N7 was fully protonated at the transition state. This agrees with the solvent deuterium KIE, 0.43, for acid-catalyzed dAdo hydrolysis,[26,64] which indicates that there is no proton transfer at the rate-limiting (as distinct from the first irreversible) transition state, which is presumably C−N bond cleavage.[65]

The minor N3H-dAMP tautomer was examined because 3-methyl-dAdo is 3600-fold more reactive than dAdo.[66] A small fraction of N3H-dAMP could potentially contribute dispropor-

(62) Glad, S. S.; Jensen, F. *J. Phys. Chem.* **1996**, *100*, 16892−16898. Scott, A. P.; Radom, L. *J. Phys. Chem.* **1996**, *100*, 16502−16513.

(63) Berti, P. J. *Methods Enzymol.* **1999**, *308*, 355−397.
(64) York, J. L. *J. Org. Chem.* **1981**, *46*, 2171−2173.

Table 4. Calculated EIEs and KIEs for dAMP Hydrolysis[a]

			KIEs						
	EIEs (D_N*$P^{\ddagger}$+A_N)[b]		A_ND_N	$D_N^{\ddagger}$*A_N[c]	D_N*$A_N^{\ddagger}$[d]		80% D_N*$A_N^{\ddagger}$/ 20% D_N*$P^{\ddagger}$+A_N[e]		
isotopic label	N1H-**3** ⇌ **4** + N1H,N7H-**5**	N1H-**1** ⇌ **2** + N1H,N7H-**5**	N1H-**1**→ N1H,N7H-**6**‡	N1H-**1** → N1H,N7H-**7**‡	N1H-**1** → α-**8a**‡	N1H-**1** → α-**8b**‡	α-**8a**‡	α-**8b**‡	experimental
1′-^{14}C	0.993	0.993	1.059	1.052	1.008	1.003	1.005	1.001	1.004
9-^{15}N	1.023	1.023	1.024	1.024	1.023[f]	1.023[f]	1.023[f]	1.023[f]	1.022
6-^{15}N	1.001	1.001	1.010	1.008	1.001[f]	1.001[f]	1.001[f]	1.001[f]	0.997
7-^{15}N	0.987	0.987	0.991	0.991	0.987[f]	0.987[f]	0.987[f]	0.987[f]	0.985
1′-^{3}H	1.364	1.355	1.047	1.068	1.390	1.259	1.383	1.278	1.253
2′*S*-^{2}H	1.183	1.181	1.045	1.047	1.179	1.145	1.179	1.152	1.113
2′*R*-^{2}H	1.078	1.073	0.997	1.007	1.081	1.019	1.079	1.030	1.091
5′,5′-$^{3}H_2$[g]	1.038	1.014	1.003	0.849	1.016	1.010	1.016	1.011	1.012

[a] See Supporting Information for the reduced isotopic partition functions, Q and $Q^{\ddagger}$, used to calculate IEs. [b] Stepwise mechanism with reversible C−N cleavage (D_N step) and diffusional separation ($P^{\ddagger}$) being the first irreversible step. [c] $k_5 \gg k_4$. [d] $k_5 \ll k_4$. [e] The expected KIE for a mechanism that proceeds 80% through a D_N*$A_N^{\ddagger}$ mechanism (reversible formation of a {**2**•N1H,N7H-**5**} complex followed by irreversible water attack on **2**) and 20% through a (D_N*$P^{\ddagger}$+A_N) mechanism (with reversible formation of {**2**•N1H,N7H-**5**}, then diffusional separation). KIE = 0.2 × EIE(N1H-**1** ⇌ **2** + N1H,N7H-**5**) + 0.8 × $KIE_{DN*AN^{\ddagger}}$. [f] The leaving group is not present in the A_N TSs; therefore the KIE is equal to the EIE(N1H-**1** ⇌ **2** + N1H,N7H-**5**). [g] [5′,5′-$^{3}H_2$] was doubly labeled at the 5′ position. Experimental and calculated KIEs are reported for the doubly labeled material, not per ^{3}H.

tionately to dAMP reactivity. With N3H-dAdo as the reactive form, the calculated 9-^{15}N and 7-^{15}N KIEs, 1.015 and 0.976, did not match the experimental values (see Supporting Information). Thus, N3 protonation was not a major contributor to acid-catalyzed dAMP hydrolysis.

The calculated 6-^{15}N KIE for a D_N*$A_N^{\ddagger}$ mechanism, 1.001, was closer to the experimental value, 0.997, than the calculated A_ND_N and $D_N^{\ddagger}$*A_N values, 1.010 and 1.008, respectively.

1′-^{3}H KIE. 1′-^{3}H KIEs are large and normal for oxacarbenium ion-like transition states. Rehybridization of C1′ from sp^3 toward sp^2 and loss of steric crowding from the adenine ring increases the out-of-plane vibrational freedom.[67] The experimental 1′-^{3}H KIE was 1.253, near the upper end of the range of previously observed 1′-hydron KIEs for nonenzymatic reactions, 1.19[2] to 1.26,[4] and the middle of the range for enzymatic reactions, 1.15 to 1.34 (e.g., see ref 17). The calculated 1′-^{3}H KIEs were somewhat higher than the experimental value and were sensitive to the position of the water nucleophile, being 1.38 for α-**8a**‡ and 1.28 for α-**8b**‡. This environmental sensitivity is consistent with the difficulties encountered previously in providing detailed interpretations of α-secondary hydron KIEs.[19,67]

Stereospecific 2′-^{2}H KIEs. The experimental 2′*S*-^{2}H and 2′*R*-^{2}H KIEs, 1.113 and 1.091, respectively, were similar to those observed previously for deoxyribosyl reactants, namely 1.102 and 1.106 for UDG[11] and 1.117 and 1.146 for ricin with DNA.[12] The main contributor to β-secondary ^{2}H KIEs in cationic transition states is hyperconjugation, i.e., donation of electron density from the C2′−H2 σ-bonds into the empty p-orbital at C1′, forming a C2′−C1′ π-bond and weakening the σ-bond. Hyperconjugation is strongly angle dependent, varying as $\cos^2 \theta_{H2'}$, where $\theta_{H2'}$ is the p-orbital−C1′−C2′−H2′ dihedral angle.[68] It is maximal at $\theta_{H2'} = 0°$ and 180°, and zero at 90°. Compound 3-*exo*-**2** had $\theta_{H2'S} = 17°$ and $\theta_{H2'R} = 44°$, with the calculated

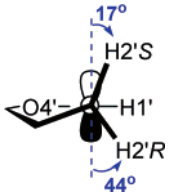

Figure 4. Oxacarbenium ion model showing the dihedral angles $\theta_{H2'}$ (∠p-orbital−C1′−C2′−H2′) in 3′-*exo*-**2**.

2′*S*-^{2}H KIE larger than that for 2′*R*-^{2}H (Figure 4). The experimental 2′*S*-^{2}H KIE was also larger than that for 2′*R*-^{2}H, though the difference was smaller than that with the calculated KIEs. This shows that the A_N transition state was a 3′-*exo* conformer. Converting the reactant's 2′-*endo* conformer to 3′-*exo* requires only facile rotations about the C1′−C2′ and O4′−C4′ bonds.

Nonenzymatic ribonucleoside hydrolysis proceeds through 3′-*exo* conformations,[2,8] as do most enzymatic reactions.[4,6,8] No conformational preference is evident from the enzymatic deoxynucleoside transition states: The stereospecific 2′-^{2}H KIEs for UDG were large and almost equal,[11] indicating a flattened deoxyribosyl ring with $\theta_{H2'S} \approx \theta_{H2'R}$, in agreement with the crystal structures.[69] In ricin-catalyzed DNA hydrolysis the 2′*R*-^{2}H KIE was larger than that for 2′*S*-^{2}H,[12] indicating a 3′-*endo* conformation, as observed for the RNA reaction.[5] The present study shows that the deoxyribo-oxacarbenium ion has an intrinsic preference for the 3′-*exo* conformer, like the ribo-oxacarbenium ion.

5′,5′-$^{3}H_2$ KIE. The experimental 5′,5′-$^{3}H_2$ KIE, 1.012, was similar to acid-catalyzed AMP hydrolysis, 1.006.[8] The calculated IE for the 5′-phosphate models (N1H-**3** → **4**) was 1.038, likely reflecting an electrostatic interaction in the gas-phase calculations between the 5′-phosphate and the positive charge at C1′. This would be screened in solution, lessening the KIE. The 5′-

(65) Solvent deuterium KIEs were measured under noncompetitive conditions; i.e., rates were measured in the presence of pure H_2O or D_2O, not a combination of both. Noncompetitive KIEs reflect the rate-limiting step of a reaction, rather than the first irreversible step. *A priori*, the rate-limiting step in dAMP hydrolysis might be expected to be N7 protonation or C−N bond cleavage. The inverse solvent deuterium KIE demonstrates that it is the latter.

(66) Fujii, T.; Saito, T.; Nakasaka, T. *Chem. Pharm. Bull.* **1989**, *37*, 2601−2609.

(67) Matsson, O.; Westaway, K. C. *Adv. Phys. Org. Chem.* **1998**, *31*, 143−248.

(68) Defrees, D. J.; Taagepera, M.; Levi, B. A.; Pollack, S. K.; Summerhays, K. D.; Taft, R. W.; Wolfsberg, M.; Hehre, W. J. *J. Am. Chem. Soc.* **1979**, *101*, 5532−5536. Sunko, D. E.; Szele, I.; Hehre, W. J. *J. Am. Chem. Soc.* **1977**, *99*, 5000−5004.

(69) Parikh, S. S.; Mol, C. D.; Slupphaug, G.; Bharati, S.; Krokan, H. E.; Tainer, J. A. *EMBO J.* **1998**, *17*, 5214−5226. Parikh, S. S.; Walcher, G.; Jones, G. D.; Slupphaug, G.; Krokan, H. E.; Blackburn, G. M.; Tainer, J. A. *Proc. Natl. Acad. Sci. U.S.A.* **2000**, *97*, 5083−5088. Bianchet, M. A.; Seiple, L. A.; Jiang, Y. L.; Ichikawa, Y.; Amzel, L. M.; Stivers, J. T. *Biochemistry* **2003**, *42*, 12455−12460.

hydroxy models (N1H-**1** → α-**8a/b**‡) gave a better match, 1.011−1.016.

Large 1′-^{14}C KIE for a Stepwise Mechanism. The calculated 1′-^{14}C KIE for a $D_N^{‡}$*A_N mechanism (N1H-**1** → N1H,N7H-**7**‡) was 1.052. This was close to the calculated value for the A_ND_N transition state, 1.059, and much higher than experimental and most calculated values previously reported for stepwise reactions,[5,9−12,70] except one computational study of AMP hydrolysis, which indicated that a 1′-^{14}C KIE of 1.045 was possible in a $D_N^{‡}$*A_N mechanism.[23] In contrast, the calculated KIE with a neutral reactant and monoprotonated transition state, i.e., **1** → N7H-**7**‡, was 1.012 (see Supporting Information), in the expected range for a stepwise mechanism. These are the protonation states that might be expected for an enzyme-catalyzed reaction at neutral pH.

The difference in 1′-^{14}C KIEs arose from differences in adenine protonation. This is most easily explained in terms of the reverse reaction. N7H-adenine is a good nucleophile; the barrier to attack on the oxacarbenium ion is overcome almost as soon as the two molecules make contact, as shown by the low C1′−N9 bond order at the transition state, $n_{C1'-N9} = 0.02$.[71] N1H,N7H-adenine is a weaker nucleophile, and there is electrostatic repulsion with the oxacarbenium ion. Thus, the TS bond order is higher, $n_{C1'-N9} = 0.18$. This is reflected in the imaginary frequencies, 30*i* versus 153*i* cm^{-1}, respectively, and contributions from the reaction coordinate motion, $^{light}\upsilon^*/^{heavy}\upsilon^* = 1.005$ and 1.024.

The computational model of ricin-catalyzed DNA hydrolysis had a neutral imidazole leaving group (**10**‡).[12] This is a reasonable representation of an N7H-monoprotonated but not an N1H,N7H-diprotonated leaving group. Similarly, monoprotonated adenine in the MTAN TS structure gave a low 1′-^{14}C KIE.[9] The influence of N1 protonation on the 1′-^{14}C KIE, five bonds away, illustrates the value of using as complete computational models as possible.

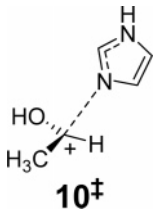

10‡

More significantly, it will not always be possible to distinguish A_ND_N from $D_N^{‡}$*A_N mechanisms. The calculated KIEs for A_ND_N and $D_N^{‡}$*A_N transition states (Table 4) are similar enough that it would not be possible to distinguish between these transition states. It still appears to be true that very small 1′-^{14}C KIEs can arise only from stepwise mechanisms; however, a 1′-^{14}C KIE ≥ 1.025, previously taken as evidence for an A_ND_N mechanism, may occasionally occur in a stepwise mechanism. Stepwise reactions with unusually stable or cationic leaving groups can result in a high leaving group bond order, n_{C-LG}, and correspondingly large primary carbon KIEs. The same will hold true for poor nucleophiles. In this context, it may be necessary to consider the possibility that nonenzymatic AMP and NAD$^+$ hydrolyses are stepwise rather than concerted.

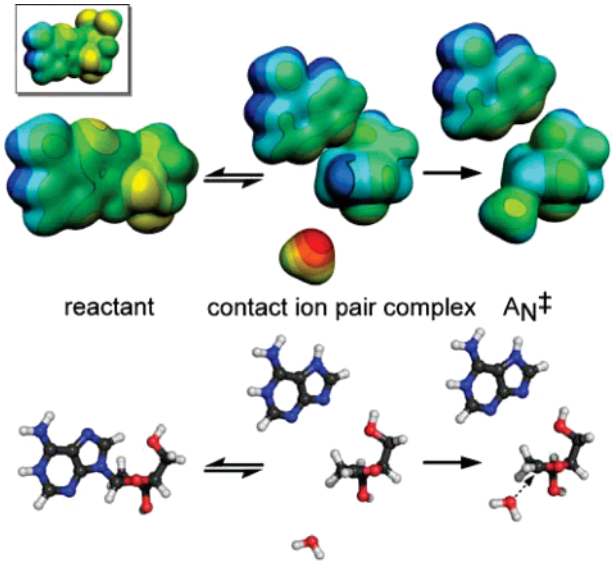

Figure 5. Structures of the dAdo reactant (N1H-**1**), CIPC (**2**•N1H,N7H-**5** + H_2O), and A_N TS structure (α-**8a**‡ + N1H,N7H-**5**). (Top) Electrostatic potential surfaces. (Inset) N1H-dAMP, showing the minimal effect of the 5′-phosphate group on the rest of the molecule. (Bottom) Atomic models of the model compounds. Molecular surfaces were plotted at an electron density of 0.002 *e*/*b*^{3}, with electrostatic potentials from negative (red, −0.08 hartree) to positive (blue, 0.28 hartree). Individual molecules in the CIPC, i.e., **2**, N1H,N7H-**5**, and H_2O, were optimized separately and brought together in the figure.

D_N*$A_N^{‡}$ Transition State. The experimental KIEs reflected water attack on an oxacarbenium ion (Figure 5). In α-**8a**‡ and *β*-**8b**‡ (and *β*-**8**‡), the nascent C1′−O bond is very weak, with bond lengths of 2.83 and 2.32 Å, corresponding to $n_{C1'-O}$ = 0.01 and 0.06, respectively. The low $n_{C1'-O}$'s reflect the high oxacarbenium ion reactivity; the transition state is reached almost as soon as the bond starts to form. The TS structures are oxacarbenium-ion-like, with only slight decreases in charge delocalization to the ring oxygen and hyperconjugation, as reflected by decreased $n_{C1'-O4'}$ and $n_{C1'-C2'}$ and increased $n_{C1'-H2S'}$ and $n_{C1'-H2R'}$. The C1′ geometry reflects the beginnings of rehybridization from sp^2 to sp.[3]

dAMP will be hydrolyzed through the N7H monoprotonated form at physiological pH (by analogy to dAdo).[17] The mechanism likely remains D_N*$A_N^{‡}$. N7H-adenine is a better nucleophile than N1H,N7H-adenine, making *N*-glycoside bond reformation in the CIPC even more likely that with the diprotonated form.

Intermediate Lifetime. The time scale for diffusional separation of an ion pair complex is 10^{-10}−10^{-11} s and is 10^{-11} s for solvent reorganization to allow *β*-attack.[29,72] If 20% of the reaction occurs after CIPC dissociation, its lifetime must be on the same order. Nucleophile selectivity also probes the intermediate lifetime. Unstable intermediates react indiscriminately, giving $k_{MeOH}/k_{H_2O} = 1$. Stable intermediates are selective, e.g.,

(70) Parkin, D. W.; Schramm, V. L. *J. Biol. Chem.* **1984**, *259*, 9418−9425.
(71) Pauling bond order is defined as $n_{ij} = e^{(r_1 - r_{ij})/0.3}$, where r_{ij} is the bond length between atoms *i* and *j* and r_1 is the bond length for a single bond between atoms of elements *i* and *j*. Single bond lengths were C−C, 1.526 Å; C−N, 1.475 Å; C−O, 1.41 Å; and C−H, 1.09 Å. (a) Johnston, H. S. *Gas Phase Reaction Rate Theory*; Ronald Press, Co.: New York, 1966. (b) Sims, L. B.; Lewis, D. E. In *Isotope Effects: Recent Developments in Theory and Experiment*; Buncel, E., Lee, C. C., Eds. Elsevier: New York, 1984; Vol. 6, pp 161−259.
(72) Richard, J. P.; Jencks, W. P. *J. Am. Chem. Soc.* **1984**, *106*, 1373−1383. Eigen, M. *Angew. Chem., Int. Ed. Engl.* **1964**, *3*, 1−19. Kaatze, U. *J. Chem. Eng. Data* **1989**, *34*, 371−374.

$k_{MeOH}/k_{H_2O} = 20$ for a carbocation with a 10^{-8} s lifetime.[73] The dAMP reaction gave $k_{MeOH}/k_{H_2O} = 1.4$, comparable with 1.1−1.6 for the oxacarbenium ions of deoxyglucose[29] and *N*-acetylneuraminate[49] in 50% MeOH, which have lifetimes of (1 to ≥3) × 10^{-11} s. Thus, by two measures, the oxacarbenium ion intermediate lifetime is on the order of 10^{-11}−10^{-10} s.

Biological Relevance. Most enzymatic reactions with 2′-hydroxynucleoside substrates proceed through highly dissociative A_ND_N TSs or, occasionally, through stepwise D_N*A_N mechanisms. Although a variety of catalytic strategies have been proposed, including leaving group or nucleophile activation, and oxacarbenium ion stabilization (see ref 17), they all appear to stabilize similar TS structures. In contrast, enzymatic 2′-deoxynucleoside reactions have wildly divergent TS structures. Ricin-catalyzed DNA hydrolysis[12] was reported to be stepwise, and UDG-catalyzed uracil hydrolysis[11] was probably stepwise. Based on the more complete computational models in the present study, the ricin and UDG KIEs match best to a $D_N^{\ddagger}$*A_N mechanism, with C−N bond cleavage being the first irreversible step (with the caveat that UDG has a pyrimidine substrate, in contrast to our purine models). In order to make C−N bond cleavage irreversible, it would be necessary to either stabilize or sequester the leaving group and/or have the water nucleophile poised for attack. In striking contrast, thymidine phosphorylase catalyzed arsenolysis proceeded through an almost synchronous A_ND_N transition state with no cationic character.[14]

While the present study demonstrates that the intrinsic reactivity of dAMP favors a stepwise mechanism with reversible oxacarbenium ion formation, it appears that enzymes have great latitude to modify the mechanism.

Summary

Acid-catalyzed dAMP hydrolysis proceeded through a stepwise mechanism, forming a discrete {oxacarbenium ion•adenine} intermediate. The experimental KIEs and anomeric product distribution demonstrated that the mechanism is ∼80% D_N*$A_N^{\ddagger}$, with reversible C−N bond cleavage, followed by irreversible water addition. About 20% proceeds through a D_N*$P^{\ddagger}$+A_N mechanism, with intermediate dissociation being the first irreversible step. Methanolysis reactions indicate that the oxacarbenium ion intermediate has a lifetime of 10^{-11}−10^{-10} s. The calculated primary KIEs depended strongly on the protonation state of the adenine leaving group. The N1H,N7H-diprotonated form gave a calculated 1′-^{14}C KIE for a $D_N^{\ddagger}$*A_N mechanism in the range normally associated with concerted A_ND_N mechanisms.

Acknowledgment. We thank Drs. Joanne Stubbe, Vern Schramm, and Bjarne Hove-Jensen for bacterial cultures that overexpressed RTRase, APRTase, and PRPPase. We thank Dr. Don Hughes and Brian Sayer (McMaster University) for NMR experiments and Dr. Kirk Green (McMaster University) for assistance in running MS analyses, Bryan Davies for assistance in synthesizing labeled adenines, and Amanda Ramnarine for help in measuring the 6-^{15}N KIE. This work was supported by the Natural Sciences and Engineering Research Council of Canada, as well as a graduate scholarship from the Natural Sciences and Engineering Research Council of Canada (J.A.B.).

Supporting Information Available: Complete citation for ref 43; ^{1}H NMRs of α- and β-Med-RMP; rate constants for dRMP, α-, and β-Me-dRMP solvolysis; complete tables for IE calculations; summary of sugar ring geometry for oxacarbenium ions; KIEs for N1H,N7H-**7**‡ and N7H-**7**‡; Cartesian coordinates for optimized structures. This material is available free of charge via the Internet at http://pubs.acs.org.

JA067371L

(73) Richard, J. P.; Rothenberg, M. E.; Jencks, W. P. *J. Am. Chem. Soc.* **1984**, *106*, 1361−1372.